Time-Resolved Linear Dichroism and Linear Birefringence of Bacteriorhodopsin at Alkaline pH: Identification of Two N Substates with Different Orientations of the Transition Dipole Moment

Berthold Borucki,* Harald Otto, and Maarten P. Heyn

Biophysics Group, Physics Department, Freie Universität Berlin, Arnimallee 14, D-14195 Berlin, Germany

Received: June 12, 2003; In Final Form: September 28, 2003

Transient linear dichroism and linear birefringence changes in the photocycle of bacteriorhodopsin at alkaline pH were measured with magnetically oriented purple membrane samples using the method of isotropic excitation (Borucki, B.; Otto, H.; Heyn, M. P. *J. Phys. Chem. B* **1999**, *103*, 6371−6383). At pH 10.4, the accumulation of the O intermediate is negligible, and N is the only intermediate that is relevant in the M decay and the recovery of the bR ground state. We introduced a new analytical approach that is model-independent and makes use of the transient linear dichroism in combination with isotropic absorbance changes. SVD analysis reveals that only one species (spectral component), namely, the N intermediate, is involved in the M decay at pH 10.4. The spectrum of this intermediate and its average anisotropy are determined from an eigenvalue equation. The transient linear dichroism data suggest a transition between two substates of the N intermediate with different anisotropies (i.e., with different orientations of the electronic transition dipole moment). Assuming that the polar angle of the transition dipole moment with respect to the membrane normal is 70° in the bR ground state, we get 66.3° (upper limit) for the first and 67.9° (lower limit) for the second N substate. The reorientation of the chromophore in the $N_1 \rightarrow N_2$ transition is probably associated with the movement of the protonated Schiff base away from Asp96, suggesting that it serves as a reprotonation switch for Asp96 by stabilizing the protonation state of the Schiff base. In contrast to measurements at neutral pH, the linear birefringence changes at alkaline pH contain a wavelength-independent component that is not due to the transient absorption changes and whose time dependence is correlated with the kinetics of the N intermediate. This result is attributed to an electro-optical effect caused by the large electric field generated by the transient negative charge on Asp96 in the N intermediate. Alternatively this change in Δn may be due to the major conformational change in the cytoplasmic region of the membrane during N.

Introduction

The light-driven proton pump bacteriorhodopsin undergoes a photocycle that is initiated by a fast isomerization of the all-trans retinylidene chromophore to a 13-cis,15-anti conformation.[1] The thermal relaxation to the initial state is accompanied by protonation changes as well as structural rearrangements of the chromophore and the protein. The sequence of these processes is characterized spectroscopically, defining photocycle intermediates (J, K, L, M, N, O) that differ in their absorption spectra in the UV−vis (λ_{max} values of 410, 560, and 630 nm for the M, N, and O intermediates, respectively, which are relevant to this study). For a recent review, see ref 2. Conformational changes of the (retinylidene) chromophore are associated with reorientations of the electronic transition dipole moment, which can be monitored by linear dichroism. Various modifications of this method, reviewed in ref 3, have been used to determine the reorientations during the bR photocycle.

In ref 4, we introduced a new experimental approach in which an oriented sample is excited isotropically. This method was further improved by an experimental arrangement of two parallel polarizers and the sample in between[5] that allows the acquisition of polarized absorption changes with high accuracy.[6] In addition to the transient absorption changes and the transient linear dichroism, the experimental data also include the transient linear birefringence changes.[6] To resolve intermediates of photochromic proteins that overlap kinetically and spectrally, we developed a formalism that was based on the combination of transient absorbance and transient linear dichroism.[6] Using a few reasonable constraints, we were able to determine the spectra and the anisotropies of the K, L, and M intermediates in the bR photocycle.[6] Only small orientational changes for the electronic transition dipole moment were derived from the anisotropies ($\Delta\theta_K \approx -0.8°$, $\Delta\theta_L \approx -1.7°$, $\Delta\theta_M \approx -1.1°$), indicating that the polar angle of the electronic transition dipole moment with respect to the membrane normal is smaller in the intermediates than in the bR ground state.[6] Our interpretation of these results—that the C_5-C_{13} part of the polyene chain tilts out of the membrane plane (see, for example, Figure 1 of ref 3)—is consistent with the recently published structures of the bR ground state and the M state at atomic resolution.[7,8] It is of particular interest to apply this method to the N intermediate as well because the M to N transition, which is spectroscopically characterized by the reprotonation of the Schiff base from Asp96,[9,10] is accompanied by major structural changes. For purple membranes, the evidence for these conformational changes comes from low-resolution X-ray diffraction,[11,12] electron paramagnetic resonance,[13,14] electron cryocrystallography,[15] and FTIR.[16−20] These conformational changes are restricted to the cytoplasmic side of the membrane and involve

* Corresponding author. E-mail: borucki@physik.fu-berlin.de. Phone: 49-30-838-55191. Fax: 49-30-838-56299.

10.1021/jp035679i CCC: $27.50
Published on Web 01/20/2004

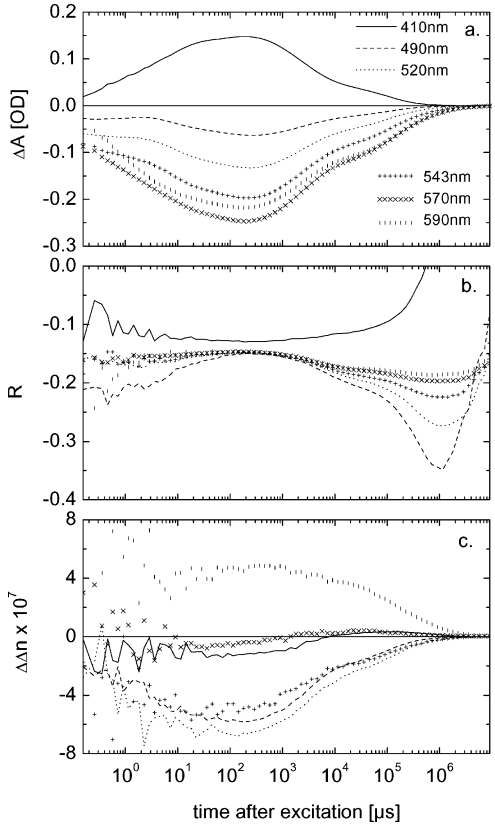

Figure 1. Time traces determined from $\Delta A(\lambda, \theta, t)$ using eq 2 and six selected wavelengths: $\lambda = 410$, 490, 520, 543, 570, and 590 nm. (a) $\Delta A(\lambda, t)$, isotropic absorbance changes; (b) $R(\lambda, t)$, anisotropy; (c) $\Delta\Delta n(\lambda, t)$, linear birefringence changes.

at least a tilt of helix F and the opening of a water-accessible channel,[12,14,15,21] which lowers the pK_a of Asp96[22] and catalyzes the reprotonation of the Schiff base. In addition, a rotation of helix F correlating with the rise of the N state has been monitored with spin-labeling ESR spectroscopy.[23] Similar changes to those in wild type have been reported for a late M intermediate in the photocycle of the mutant D96N,[24−28] suggesting that this state (M_N) is in an N-like conformation but with a deprotonated Schiff base characterizing the M intermediate. Several studies came to the conclusion that the substantial structural changes in wild type likewise already appear between two M substates rather than in the formation of the N intermediate.[21,29−35] In the M_N state of 3D crystals of D96N, the cytoplasmic parts of helices E, F, and G are disordered.[2,8,15] In a very recent study, the crystal structure of a photostationary state of the mutant V49A has been determined to 1.62 Å resolution; this state has been attributed to a late N intermediate with reprotonated Asp96.[36] The absence of large-scale conformational changes in this state suggests that the reprotonation of Asp96 might have initiated the recovery of the initial protein conformation.[36]

For spectroscopic studies on wild-type bR at neutral pH, investigations on the N intermediate are difficult because of the low accumulation and the strong temporal overlap with the O intermediate.[10,37,38] Moreover, there is also strong spectral overlap because the absorption spectrum of the N intermediate is very similar to that of the bR ground state. At high pH (>pH 10), however, the contribution of the O intermediate is negligible, and the N intermediate is the only intermediate that is involved in the decay of M and the recovery of the bR ground state. However, under these conditions, the kinetics of the M decay is multiphasic—a large number of exponentials is required for a satisfactory fit[39]—and the formalism that we applied successfully to the early part of the photocycle is not appropriate. Therefore, we developed a new formalism that does not require linearly independent extrapolated difference spectra of a sequence of first-order relaxation processes.[6] From the combination of the time traces of the absorbance changes and the transient linear dichroism, the time dependence was eliminated, leading to an eigenvalue equation that yields both the intermediate spectra (eigenvectors) and the related anisotropies (eigenvalues).

Materials and Methods

The orientation of purple membranes in high magnetic fields and immobilization in polyacrylamide gels were performed as described.[4,5] Using a 14-T superconducting magnet, we achieved an orientational order parameter S_2 of about 0.5. For an enhanced accumulation of the N intermediate in the bR photocycle, the sample was equilibrated in a 20 mM $NaHCO_3/Na_2CO_3$ buffer at pH 10.4 (150 mM KCl).

Steady-state and time-resolved polarized absorption measurements were performed as described previously.[5,6] The essential feature of our measuring scheme is that the oriented sample is placed between two parallel polarizers. The transmitted intensity of this setup measured as a function of the polarization angle (i.e., the angle between the orientation axis of the sample and the transmission axis of the polarizers) allows us to determine the isotropic absorbance, linear dichroism, and linear birefringence with high accuracy. Transient changes in these quantities were obtained from the analogous time-resolved measurements, where the sample was excited isotropically with quasi-saturating intensity. To prevent photoreactions from the slowly decaying components in the bR photocycle at alkaline pH (the recovery of the bR ground state is completed in about 10 s), the intensity of the measuring beam was reduced to about 20%, with respect to measurements at standard conditions, in the wavelength range of 520 nm $< \lambda <$ 650 nm. Because photobleaching occurs at high pH to a greater extent than at neutral pH, we reduced the total number of flashes by measuring transient changes at 13 wavelengths (390, 410, 430, 460, 490, 520, 543, 570, 590, 610, 635, 650, and 670 nm) at only 3 polarization angles ($\theta = 0$, 45, 90°). Additional measurements at 8 polarization angles ($\theta = -20$, 0, 20, 40, 50, 70, 90, 110°) were carried out at $\lambda =$ 490, 520, 543, and 570 nm, where we expect a relatively high contribution from the N intermediate to the signal. Each time trace $\Delta A(\lambda, \theta, t)$ is an average over 30 flashes. A total of 3500 flashes were required, including additional control measurements. Absorption spectra measured before and after the flash experiments show a decrease in absorbance of about 5%. The data were corrected for this bleaching effect. The polarized absorbance data $\Delta A(\lambda, \theta, t)$ were averaged in time so that 10 equally spaced logarithmic data points were resolved in each time decade.

Data Analysis

The formalism presented here has the same starting point as the data analysis that we developed previously for the early intermediates in the bR photocycle.[6] For a better understanding, we summarize briefly the main previous equations and then present the novel aspects.

In our time-resolved experiments, the absorbance change at polarization angle θ, wavelength λ, and time after excitation t is calculated directly from the signal (transmitted intensity) before the flash $I(\lambda, \theta, t_0)$ and the time course of the signal after the excitation $I(\lambda, \theta, t)$:

$$\Delta A(\lambda, \theta, t) := \log\frac{I(\lambda, \theta, t_0)}{I(\lambda, \theta, t)} \quad (1)$$

We derived previously[6] that $\Delta A(\lambda, \theta, t)$ depends in the following way on the steady-state parameters $E_0(\lambda)$ (isotropic extinction), $r_E(\lambda)$ (related anisotropy), and $\Delta\phi_E(\lambda)$ (phase difference) and on the transient quantities $\Delta A(\lambda, t)$ (isotropic absorbance change), $R(\lambda, t)$ (anisotropy), and $\Delta\phi_E(\lambda, t)$ (phase difference due to linear birefringence changes):

$$\begin{aligned}\Delta A(\lambda, \theta, t) = \Delta A(t)(1 - R(t)) \\ + \log[\cos^4\theta\, 10^{-3E_0 r_E} + \sin^4\theta + \\ 2\cos^2\theta \sin^2\theta\, 10^{-3/2E_0 r_E}\cos(\Delta\phi_E)] \\ - \log[\cos^4\theta\, 10^{-3(E_0 r_E + \Delta A(t)R(t))} + \sin^4\theta \\ + 2\cos^2\theta \sin^2\theta\, 10^{-3/2(E_0 r_E + \Delta A(t)R(t))} \\ \cos(\Delta\phi_E(t))] \quad (2)\end{aligned}$$

For clarity, the wavelength dependence on the right-hand side of this equation is suppressed. Whereas $\Delta A(\lambda, t)$ and $R(\lambda, t)$ arise directly from the measurements at polarization angles $\theta = 0$ and 90° ($\Delta A(0°) = \Delta A(1 + 2R)$, $\Delta A(90°) = \Delta A(1 - R)$), the determination of the transient quantity $\Delta\phi_E(\lambda, t)$ from eq 2 requires that the steady-state parameters $E_0(\lambda)$, $r_E(\lambda)$, and $\Delta\phi_E(\lambda)$ be known. For the steady-state measurements, we refer to refs 5 and 6. In principle, only one additional measurement at a polarization angle θ (i.e., $\theta = 45°$) is necessary to determine $\Delta\phi_E(\lambda, t)$ from eq 2 with $\Delta A(\lambda, t)$ and $R(\lambda, t)$ analytically. Higher accuracy is obtained by fitting $\Delta A(\lambda, \theta, t)$ at more than three polarization angles θ with the expression on the right side of eq 2, varying the three transient parameters $\Delta A(\lambda, t)$, $R(\lambda, t)$, and $\Delta\phi_E(\lambda, t)$.

Instead of the transient change in the phase difference $\Delta\Delta\phi(\lambda, t) = \Delta\phi_E(\lambda, t) - \Delta\phi_E(\lambda)$, we consider the transient linear birefringence change

$$\Delta\Delta n(\lambda, t) = \frac{\Delta\Delta\phi(\lambda, t)}{2\pi} \cdot \frac{\lambda}{d} \quad (3)$$

which is physically more relevant. The chromophore contribution of $\Delta\Delta n(\lambda, t)$ is related to the transient linear dichroism $\Delta A(\lambda, t)\, R(\lambda, t)$ by the Kramers−Kronig transform:

$$\Delta\Delta n(\lambda, t) = \frac{3\ln 10}{2\pi^2 d} P\int_0^\infty \frac{\Delta A(\lambda', t)\, R(\lambda', t)}{\left(1 - \frac{\lambda'}{\lambda}\right)\left(1 + \frac{\lambda'}{\lambda}\right)} \mathrm{d}\lambda' \quad (4)$$

This equation is used to determine whether the measured transient linear dichroism and the transient birefringence changes are consistent. For the determination of the intermediate spectra A_i and their anisotropies r_i, we use only the absorbance changes $\Delta A(\lambda, t)$ and the transient linear dichroism $\Delta A(\lambda, t)\, R(\lambda, t)$. In ref 6, we introduced a matrix formalism that conveniently describes the further steps in the data analysis.

$$\Delta\mathbf{A} = (\mathbf{A} - \mathbf{A_{bR}})\mathbf{n} \quad (5)$$

$$\Delta\mathbf{AR} = (\mathbf{AD}_i - \mathbf{A_{bR}D}_{bR})\mathbf{n} \quad (6)$$

where the column index of $\Delta\mathbf{A}$, $\Delta\mathbf{AR}$, and $\mathbf{n}$ corresponds to the time t (i.e., the rows of $\mathbf{n}$ are the time courses of the intermediates). The row index of $\Delta\mathbf{A}$, $\Delta\mathbf{AR}$, $\mathbf{A}$, and $\mathbf{A}_{bR}$ corresponds to the wavelength λ, and the column index of $\mathbf{A}$ and $\mathbf{A}_{bR}$ corresponds to the intermediate i. Matrix $\mathbf{A}_{bR}$ consists of identical columns. $\mathbf{D}_i$ and $\mathbf{D}_{bR}$ are diagonal matrices with elements r_i and r_{bR}, respectively, where $\mathbf{D}_{bR} = r_{bR}\mathbf{I}$. This formalism implicitely uses the assumption of wavelength-independent anisotropies r_i and r_{bR}.

Generally in eqs 5 and 6, the spectra $\mathbf{A}$, the anisotropies r_i, and the time courses $\mathbf{n}$ of the intermediates have to be considered to be unknown parameters. In our previous work,[6] we used a fit of the evolution in time with exponentials and/or power laws and eliminated the matrix of the intermediate spectra $\mathbf{A}$ from eqs 5 and 6. Here we eliminate the matrix of the intermediate time courses $\mathbf{n}$ from this pair of equations, which requires that we first carry out the singular value decomposition[40,41] (SVD) of the combined array of absorbance changes ($\Delta\mathbf{A}$) and transient linear dichroism ($\Delta\mathbf{AR}$):

$$\begin{pmatrix}\Delta\mathbf{A} \\ \Delta\mathbf{AR}\end{pmatrix} = \begin{pmatrix}\mathbf{U} \\ \mathbf{U}^R\end{pmatrix}\mathbf{D}_s\mathbf{V} \quad (7)$$

The colums of $\mathbf{U}$ and $\mathbf{U}^R$ represent the basis spectra of the absorption changes $\Delta\mathbf{A}$ and the transient linear dichroism $\Delta\mathbf{AR}$, respectively; the rows of $\mathbf{V}$ are the related time courses, and $\mathbf{D}_s$ is the diagonal matrix of the singular values. Using this SVD representation, eqs 5 and 6 become

$$\mathbf{UD}_s\mathbf{V} = (\mathbf{A} - \mathbf{A_{bR}})\mathbf{n} \quad (8)$$

$$\mathbf{U}^R\mathbf{D}_s\mathbf{V} = (\mathbf{AD}_i - \mathbf{A_{bR}D}_{bR})\mathbf{n} \quad (9)$$

Multiplication by $\mathbf{U}^{-1}$, the pseudoinverse of $\mathbf{U}$, from the left solves eq 8 for $\mathbf{D}_s\mathbf{V}$, which is subsequently inserted into eq 9:

$$\mathbf{U}^R\mathbf{U}^{-1}(\mathbf{A} - \mathbf{A_{bR}})\mathbf{n} = (\mathbf{AD}_i - \mathbf{A_{bR}D}_{bR})\mathbf{n} \quad (10)$$

Multiplication by $\mathbf{n}^{-1}$, the pseudoinverse of $\mathbf{n}$, from the right and a rearrangement yield

$$\mathbf{U}^R\mathbf{U}^{-1}\mathbf{A} - \mathbf{AD}_i = \mathbf{U}^R\mathbf{U}^{-1}\mathbf{A}_{bR} - \mathbf{A}_{bR}\mathbf{D}_{bR} \quad (11)$$

Similar to the previous formalism, in this matrix equation the columns of the matrices $\mathbf{A}$ representing the intermediate spectra are decoupled. Equation 11 turns into a vector equation that has to be satisfied by each column $(\mathbf{A})_i = \vec{A}_i$ and the related anisotropy r_i.

$$(\mathbf{U}^R\mathbf{U}^{-1} - r_i\mathbf{I})\vec{A}_i = (\mathbf{U}^R\mathbf{U}^{-1} - r_{bR}\mathbf{I})\vec{A}_{bR} \quad (12)$$

In general, if the right side of eq 12 does not equal the null vector, then this vector equation is an underdetermined nonlinear system of equations. For any given value r_i, the corresponding vector $\vec{A}_i$ may be determined. However, eq 12 is very useful if we consider a certain wavelength region where one intermediate does not contribute to absorption (e.g., $\vec{A}_m \equiv \vec{0}$). In this case, the left side is the null vector, and eq 12 represents an eigenvalue equation where r_{bR} is the eigenvalue of the matrix $\mathbf{U}^R\mathbf{U}^{-1}$ and $\vec{A}_{bR}$ is the corresponding eigenvector:

$$(\mathbf{U}^R\mathbf{U}^{-1} - r_{bR}\mathbf{I})\vec{A}_{bR} = \vec{0} \quad (13)$$

This equation provides a check of whether the spectrum of the bR ground state $\vec{A}_{bR}$ determined in the steady-state measurement is consistent with the transient data $\Delta\mathbf{AR}$ and $\Delta\mathbf{A}$. Because the right side of eq 12 is the null vector, it follows directly that the anisotropies r_i and the corresponding spectra $\vec{A}_i$ (of the absorbing species) have to fulfill the eigenvalue equation as well:

$$(\mathbf{U}^R\mathbf{U}^{-1} - r_i\mathbf{I})\vec{A}_i = \vec{0} \quad (14)$$

The rank of matrix $\mathbf{U}^R\mathbf{U}^{-1}$ equals the rank of $\mathbf{U}$ and $\mathbf{U}^R$; therefore, the number of eigenvalues different from zero equals the number of relevant basis spectra included in $\mathbf{U}$ and $\mathbf{U}^R$. However, the eigenvalue equation does not provide a unique solution for the spectra $\vec{A}_i$ because the scaling of the eigenvector is still a free parameter. Restrictions on this scaling factor may arise from constraints on the relative concentrations of the intermediates $\mathbf{n}$, namely, that no negative concentrations are allowed.

We note that the validity of the eigenvalue eqs 13 and 14 requires one intermediate that does not contribute to the absorption in a certain wavelength range. To overcome this restriction, the differential quantities $\Delta\mathbf{A}$ and $\Delta\mathbf{AR}$ have to be replaced by the absolute quantities $(\mathbf{A}^{abs})_t := (\Delta\mathbf{A})_t + \vec{A}_{bR}$ and $(\mathbf{AR}^{abs})_t := (\Delta\mathbf{AR})_t + r_{bR}\vec{A}_{bR}$. A joint SVD of the matrices $\mathbf{A}^{abs}$ and $\mathbf{AR}^{abs}$ according to eq 7 leads formally to the same eigenvalue equation (eq 14). The disadvantages of this approach are (1) that a wavelength-independent anisotropy is required and, more importantly, (2) that the steady-state parameters enter into the analysis. However, the anisotropy of higher absorption bands is not necessarily the same as for the main absorption band, and the steady-state parameters, at least in our experiment, cannot be determined with the same accuracy as the transient data. Therefore, we refrained from analyzing the absolute data, generated as indicated above, and considered the eigenvalue problem using the transient data ($\Delta\mathbf{A}$ and $\Delta\mathbf{AR}$) in a limited wavelength range according to eq 14.

Apart from the uncertainty in the scaling of the eigenvectors ($\vec{A}_i \equiv (\mathbf{A})_i$ and ($\vec{A}_{bR}$, $\vec{A}_{bR}$, .., $\vec{A}_{bR}$) $\equiv \mathbf{A}_{bR}$), the time courses of the intermediates, the rows of $\mathbf{n}$, arise directly from the inversion of eqs 5 and 6:

$$\mathbf{n} = (\mathbf{A} - \mathbf{A}_{bR})^{-1}\Delta\mathbf{A} \tag{15}$$

$$\mathbf{n} = (\mathbf{AD}_i - \mathbf{A}_{bR}\mathbf{D}_{bR})^{-1}\Delta\mathbf{AR} \tag{16}$$

In these equations, the wavelength range of $\Delta\mathbf{A}$ and $\Delta\mathbf{AR}$ is the same as that used in the eigenvalue eqs 13 and 14. The intermediate spectra over the measured wavelength range arises from the repeated inversion of eq 15, where the complete wavelength range of $\Delta\mathbf{A}$ has to be taken consistently:

$$\vec{A}_i = \Delta\mathbf{A}(\mathbf{n}^{-1})_i + \vec{A}_{bR} \tag{17}$$

The spectrum of the bR ground state that is also required in eq 17 was constructed by merging the eigenvector $\vec{A}_{bR}$ above 490 nm with the steady-state absorption spectrum below 490 nm. The determination of the anisotropy r_i as an eigenvalue of the matrix $\mathbf{U}^R\mathbf{U}^{-1}$ implicitely includes an averaging in wavelength and in time. In our formalism, we assumed that the anisotropy of intermediate i is independent of wavelength within one electronic absorption band and independent of time. Some algebraic transformations are useful to check whether the spectra and the anisotropies of the intermediates determined above are consistent with these assumptions. Checking the wavelength dependence of r_i, we solve eq 6 for $\mathbf{AD}_i$ and consider column i, which is analogous to the formalism we previously introduced:[6]

$$r_i\vec{A}_i = \Delta\mathbf{AR}(\mathbf{n}^{-1})_i + r_{bR}\vec{A}_{bR} \tag{18}$$

Dividing element λ on both sides of eq 18 by the corresponding absorbance $(\vec{A}_i)_\lambda$, we get r_i as a wavelength-dependent quantity:

$$(r_i)_\lambda = \frac{(\Delta\mathbf{AR}(\mathbf{n}^{-1})_i + r_{bR}\vec{A}_{bR})_\lambda}{(\vec{A}_i)_\lambda} \tag{19}$$

The weighted-average value $\bar{r}_i$ that results from the multiplication of eq 18 with the pseudoinverse $(\vec{A}_i)^{-1}$ from the right,

$$\bar{r}_i = (\vec{A}_i)^{-1}(\Delta\mathbf{AR}(\mathbf{n}^{-1})_i + r_{bR}\vec{A}_{bR}) \tag{20}$$

should equal the eigenvalue r_i provided that the same wavelength range is used. Considering the wavelength range where $\vec{A}_m \equiv \vec{0}$, analogous transformations of eq 18 yield the corresponding information about the bR ground state:

$$(r_{bR})_\lambda = -\frac{(\Delta\mathbf{AR}(\mathbf{n}^{-1})_m)_\lambda}{(\vec{A}_{bR})_\lambda} \tag{21}$$

$$\bar{r}_{bR} = -(\vec{A}_{bR})^{-1}\Delta\mathbf{AR}(\mathbf{n}^{-1})_m \tag{22}$$

Checking the time dependence of r_i, we solve eq 6 for $\mathbf{D}_i\mathbf{n}$, where the full wavelength range of $\mathbf{A}$ is required ($\vec{A}_m \neq \vec{0}$):

$$\mathbf{D}_i\mathbf{n} = \mathbf{A}^{-1}(\Delta\mathbf{AR} + \mathbf{A}_{bR}\mathbf{D}_{bR}\,\mathbf{n}) \tag{23}$$

The expression $\mathbf{D}_i\mathbf{n}$ may be considered to be the time dependence of the intermediate anisotropies that are weighted with the corresponding concentrations. Hence, the division of element (it) by $(\mathbf{n})_{it}$ yields the time dependence of the intermediate anisotropies:

$$r_{it} = \frac{[\mathbf{A}^{-1}(\Delta\mathbf{AR} + \mathbf{A}_{bR}\mathbf{D}_{bR}\,\mathbf{n})]_{it}}{(\mathbf{n})_{it}} \tag{24}$$

Results

From the polarized absorbance data $\Delta A(\lambda, \theta, t)$ at three polarization angles $\theta = 0$, 45, 90, the time traces $\Delta A(\lambda, t)$, $R(\lambda, t)$, and $\Delta\Delta n(\lambda, t)$ were calculated analytically for each wavelength λ using eqs 2 and 3. At the four wavelengths $\lambda =$ 490, 520, 543, and 570 nm, the traces $\Delta A(\lambda, t)$, $R(\lambda, t)$ and $\Delta\Delta n(\lambda, t)$ were obtained from the fitting of $\Delta A(\lambda,\theta, t)$ at eight polarization angles with eq 2. The traces that arise from both procedures (analytical vs fitting) are in good agreement, demonstrating that the experimental setup was well adjusted and that, in this case, the measurement at only three polarization angles provides sufficient accuracy.

The time traces are shown for six selected wavelengths in Figure 1. The absorbance changes $\Delta A(\lambda, t)$ (Figure 1a) show the well-known characteristics of the bR photocycle at alkaline pH. The time trace at 410 nm is diagnostic for the population of the M intermediate. Whereas the rise of the M intermediate is accelerated at pH 10.4, the decay of M is apparently multiphasic with kinetic components in the range of seconds. The maximal accumulation of M is reached at about 200 μs. No positive absorbance changes at 490 nm occurred in the time domain from 1 to 10 μs, indicating that the accumulation of the L intermediate is low under these conditions. The transient anisotropies $R(\lambda, t)$ (Figure 1b) show a clear behavior at the selected wavelengths. In good agreement with our measurements at neutral pH,[6] the anisotropy trace at 410 nm reaches a smaller absolute value than for wavelengths $\lambda \geq 490$ nm because the absolute value of the M anisotropy is smaller than the

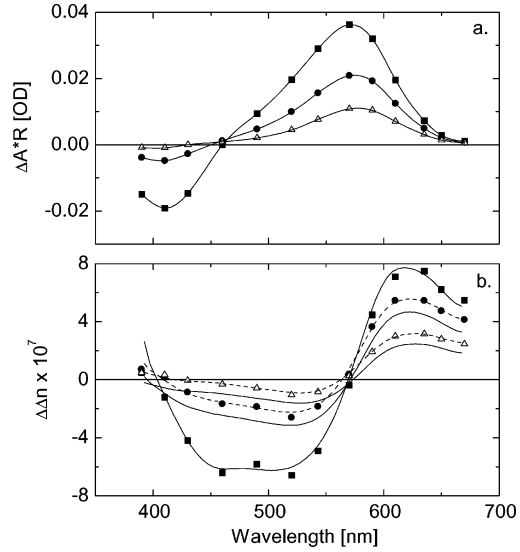

Figure 2. Spectral relationship of transient linear dichroism and linear birefringence changes. (a) Symbols: transient linear dichroism data at $t = 200\ \mu$s (■), $t = 20$ ms (●), and $t = 200$ ms (△). Lines: Spline fits of the data. (b) Symbols: data of the linear birefringence changes at $t = 200\ \mu$s (■), $t = 20$ ms, (●) and $t = 200$ ms (△). Solid lines: Kramers−Kronig transform of the spline fits in part a. Dashed lines: Kramers−Kronig transform of the spline fits in part a corrected with a constant offset ($+9 \times 10^{-8}$ for $t = 20$ ms and $+7 \times 10^{-8}$ for $t = 200$ ms).

ground-state anisotropy. For $\lambda \geq 490$ nm, the anisotropy traces reach at maximal M accumulation almost the same value ($R(\lambda, 200\ \mu s) \approx -0.147$) and obey the following relation for t between 200 μs and 1 s:

$$-0.147 > R(590\text{ nm}, t) > R(570\text{ nm}, t) > R(543\text{ nm}, t) > R(520\text{ nm}, t) > R(490\text{ nm}, t)$$

Using the approximation that only the N intermediate contributes, the transient anisotropy simplifies to $R = (A_N r_N - A_{bR} r_{bR})/(A_N - A_{bR})$. With $(A_N - A_{bR}) < 0$, the inequalities for R imply that in the late time domain one intermediate accumulates (namely, the N intermediate) whose anisotropy is smaller in absolute value than that of the bR ground state ($r_{bR} < r_N < 0$). The relation of the transient anisotropies at the different wavelengths is consistent with the ratio of the absorption values A_N/A_{bR} being maximal at 490 nm and minimal at 590 nm.

As expected from the relationship between absorption and refractive index, the transient linear birefringence data show only small changes at the wavelengths of maximal absorbance change (i.e., at 410 and 570 nm), but positive changes at 590 nm and negative changes at 490, 520, and 543 nm occur for $t \geq 10\ \mu$s (Figure 1c). Considering the relationship of birefringence changes $\Delta\Delta n(\lambda, t)$ and transient linear dichroism $\Delta A(\lambda, t)$ $R(\lambda, t)$ more quantitatively, we transform the spline fits to the linear dichroism data at the time points $t \approx 200\ \mu$s, $t \approx 20$ ms, and $t \approx 200$ ms (Figure 2a) according to eq 4 (Kramers−Kronig transform). A comparison of the transform curves and the measured birefringence changes $\Delta\Delta n(\lambda, t)$ shows good agreement for $t \approx 200\ \mu$s, but for the later time points, systematic deviations occur (Figure 2b). For $t \approx 20$ and 200 ms, the measured birefringence changes obviously have positive wavelength-independent offsets of 9×10^{-8} and 7×10^{-8}, respectively, relative to the transform curves. The shifted values of the transform curves show good agreement with the birefringence changes determined experimentally (Figure 2b). To

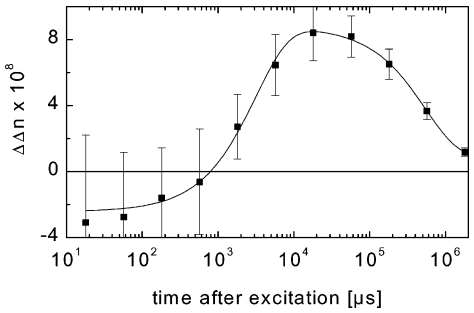

Figure 3. Kinetics of the nonabsorptive contribution to linear birefringence averaged over the spectral range from 410 to 670 nm. Symbols: data; error bars: standard deviations; line: fit with two exponentials ($\tau_1 \approx 3$ ms, $\tau_2 \approx 500$ ms).

examine the kinetics of this nonabsorptive contribution to the linear birefringence, an averaging in wavelength was carried out, and two time points per decade were selected (Figure 3). The error bars indicate the standard deviations in the averaging procedure. The time course (rise and decay) was fitted with two exponentials ($\tau_{rise} \approx 3$ ms, $\tau_{decay} \approx 500$ ms). The negative values for $t < 1$ ms are likely due to a systematic error because the determination of $\Delta\Delta\phi(\lambda, t)$ from eq 2 requires the steady-state linear birefringence $\Delta\phi_E(\lambda)$, which cannot be measured with such high accuracy. The zero value is within the standard deviation in this time domain. Considering wavelengths with large changes in linear birefringence (e.g., 610 nm), we find that the relative contribution of the nonabsorptive part is nearly negligible at 200 μs but reaches about 20% at 20 ms.

To make further progress in the data analysis, we make use only of the time traces $\Delta A(\lambda, t)$ and $\Delta A(\lambda, t)$ $R(\lambda, t)$ and assume (1) that the M intermediate does not contribute to absorption at $\lambda \geq 490$ nm and (2) that M reaches complete accumulation at $t \approx 200\ \mu$s. The latter assumption is plausible for the bR photocycle at high pH because the fraction of the L intermediate in the L−M equilibrium at maximal M accumulation decreases considerably with increasing pH (40−50% at pH 4.7 and 20% at pH 7).[6] On the basis of these assumptions, the spectrum of the bR ground state for $\lambda \geq 490$ nm is given by $\bar{A}_{bR} = -\Delta A(\lambda, 200\mu s)/\eta$, where η is the fraction of cycling molecules. The spectrum determined in this way differs slightly (but systematically) from the steady-state spectrum (Figure 4a). By chosing $\eta = 0.3$, the absorbance at 570 nm ($A_{bR}(570\text{ nm})$) coincides in the two spectra. This value of η is quite resonable. The subsequent results depend very weakly on this choice. The spectrum determined from the transient data is apparently more narrow than the steady-state spectrum, which is, however, possibly heterogeneous.

The arrays $\Delta\mathbf{A}$ and $\Delta\mathbf{AR}$ were reduced to the late time range ($t \geq 200\ \mu$s) and to rows that are related to wavelengths $\lambda =$ 490, 520, 543, 570 and 590 nm and are then combined in one matrix according to eq 7. The SVD of this combined matrix yielded the singular values $s_1 = 1.5757$, $s_2 = 0.0664$, $s_3 = 0.0044$, and so forth. Because s_3 is less than 0.3% of s_1, we consider only the first two basis spectra to be relevant contributions. Reducing $\mathbf{U}$ and $\mathbf{U}^R$ to these basis spectra (two columns), the matrix $\mathbf{U}^R\mathbf{U}^{-1}$ has the eigenvalues $r_1 = -0.1486$ and $r_2 = -0.1238$. Because the first eigenvalue r_1 is very close to the transient anisotropy at 200 μs at the wavelengths used for the calculation of $R(\lambda, 200\ \mu s) = -0.147$, we identify r_1 with r_{bR}, the anisotropy of the bR ground state, whereas the second eigenvalue r_2 is related to the N intermediate. The corresponding eigenvectors that are normalized to unit length are

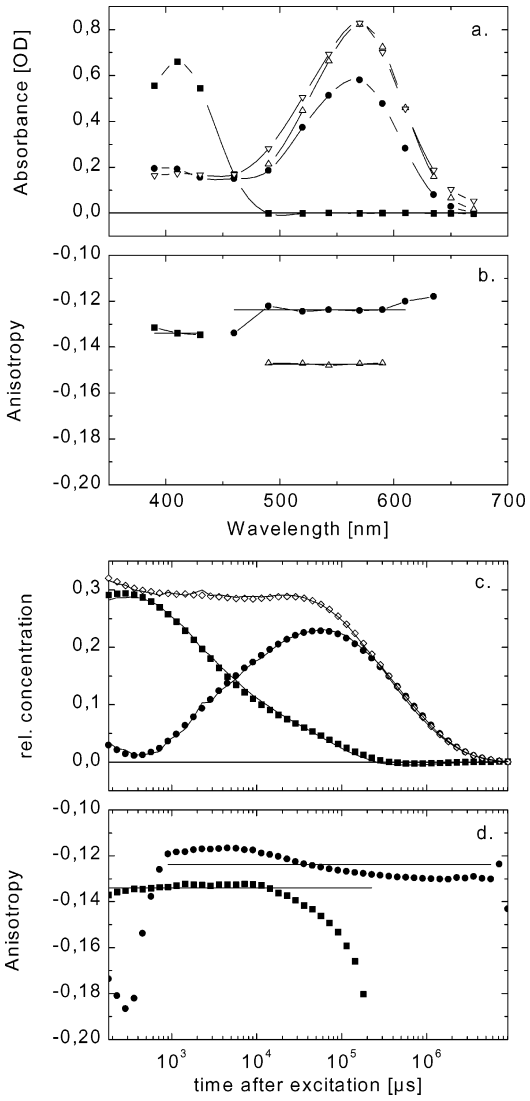

Figure 4. Results of the analysis for $|\vec{A}^*_N| = 1$: (a) intermediate spectra $\vec{A}_i$; (b) wavelength dependence of the intermediate anisotropies, symbols: $(r_i)_\lambda$, lines: $\bar{r}_i$; (c) time courses of the intermediates, symbols: calculation from $\Delta A(\lambda, t)$ according to eq 15, lines: calculation from $\Delta A(\lambda, t)$ $R(\lambda, t)$ according to eq 16; (d) time course of the intermediate anisotropies, symbols: $r_i(t)$, lines: $\bar{r}_i$. ■: M, ●: N, △: bR (from the transient data). ▽ in (a): steady-state bR spectrum; ◇ in (c): concentration sum of M and N.

$$\vec{A}^*_{bR} = \begin{pmatrix} 0.156 \\ 0.325 \\ 0.483 \\ 0.599 \\ 0.528 \end{pmatrix} \quad \text{and} \quad \vec{A}^*_N = \begin{pmatrix} 0.183 \\ 0.374 \\ 0.512 \\ 0.580 \\ 0.477 \end{pmatrix}$$

Both states have maximal absorbance at 570 nm (fourth element of the vector), but the spectrum of the N intermediate is slightly blue-shifted with respect to the bR ground state. Scaling of the eigenvector $\vec{A}^*_{bR}$ with an appropriate factor (1.373) shows nearly perfect agreement with the absorbances determined from $\Delta A(\lambda, 200\ \mu s)$. For the present, the scaling of the eigenvector $\vec{A}^*_N$ remains as indicated above. The time courses of the intermediates M and N were calculated either from eq 15 or 16 and are shown in Figure 4c. The fact that there are only small deviations between both calculations indicates that the solution of the eigenvalue equation is consistent with the data. The time course of the N intermediate for $t \leq 500\ \mu s$ is clearly unphysical, which is probably due to a small contribution of the decaying predecessor intermediate of M, namely, the L intermediate. The sum of the concentrations of M and N is nearly constant until 30 ms.

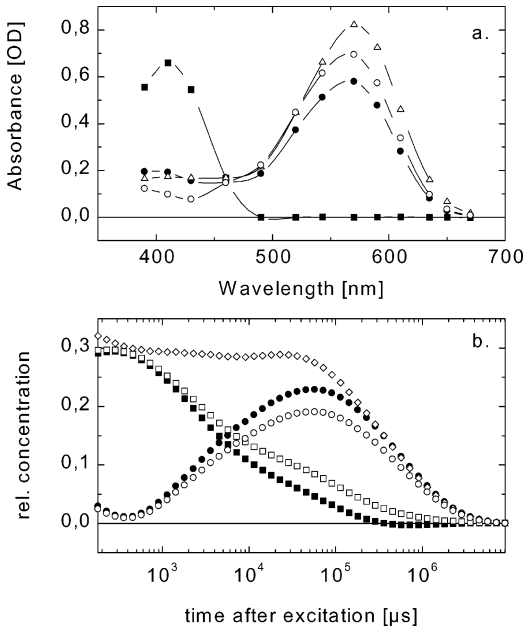

Figure 5. Influence of the scaling factor $f := |\vec{A}^*_N|$ of the eigenvector on the intermediate spectra (a) and their concentration courses (b). ■: M for $f = 1.0$; ●: N for $f = 1.0$; □: M for $f = 1.2$; ○: N for $f = 1.2$; △: bR (from the transient data); ◇ in (b): concentration sum of M and N.

The complete intermediate spectra of M and N (Figure 4a) were calculated from eq 17 after inverting the matrix of the intermediate concentrations **n**. The spectrum of the bR ground state that is also required in this calculation (eq 17) was spliced together from $A_{bR}(\lambda) = -\Delta A(\lambda, 200\ \mu s)/0.3$ above 490 nm and the steady-state absorbance values below 490 nm. The spectrum of the M intermediate, which depends on the steady-state absorbance of the bR ground state below 490 nm, is in good agreement with earlier publications.

The wavelength-dependent anisotropies calculated with eqs 19 and 21 show only small deviations from the weighted-average anisotropies according to eqs 20 and 22, respectively (Figure 4b). The average anisotropy of the N intermediate $\bar{r}_N = -0.1238$ is identical to the above-determined eigenvalue r_2; for bR there is only a small difference between the average anisotropy value of $\bar{r}_{bR} = -0.1474 \pm 0.0003$ and the eigenvalue r_1. The average anisotropy of the M intermediate is $\bar{r}_M = -0.1337 \pm 0.0013$.

The time dependence of the intermediate anisotropies according to eq 24 is shown in Figure 4d, where the horizontal lines indicate the average values determined above. The anisotropy of M is nearly constant until 10 ms, and its value is identical to $\bar{r}_M$. It diverges for longer times when the concentration of M becomes very small, most likely because of contributions of the higher absorption bands of the bR ground state and N. The anisotropy of N remains constant in the time range from 1 to 10 ms at a value above the average value $\bar{r}_N$ and reaches a value below $\bar{r}_N$ for long times. The transition occurs around 50 ms (Figure 4d). This feature will be discussed later.

In Figure 5, we compare the intermediate spectra and the related concentration courses for the scaling factors $f_1 = 1.0$ and $f_2 = 1.2$ with respect to the normalized eigenvector $\vec{A}^*_N$. To demonstrate the effect of the scaling procedure on the concentration courses, we introduce the transformation matrix **F** and its inverse $\mathbf{F}^{-1}$:

$$\mathbf{F} = \begin{pmatrix} 1 & (1-f) \\ 0 & f \end{pmatrix} \leftrightarrow \mathbf{F}^{-1} = \begin{pmatrix} 1 & (1-(1/f)) \\ 0 & 1/f \end{pmatrix}$$

From the relation

$$\Delta\mathbf{A} = (\mathbf{A} - \mathbf{A}_{bR})\mathbf{F}\mathbf{F}^{-1}\mathbf{n}$$

it follows that the transformation of $(\mathbf{A} - \mathbf{A}_{bR})$ with $\mathbf{F}$ requires $\mathbf{n}$ to be transformed with $\mathbf{F}^{-1}$. The spectrum of the M intermediate is invariant under this transformation ($(\mathbf{F})_{11} = 1$ and $(\mathbf{F})_{21} = 0$). We note that the linear scaling of the spectrum of N accomplished by this transformation affects only the spectral range, where the M intermediate does not contribute to absorption. In the short-wavelength range, up-scaling ($f > 1$) has the inverse effect (i.e., decreased absorbance). The sum of the concentrations of N and M is invariant under the transformation with $\mathbf{F}^{-1}$ and consequently provides no constraint for the scaling factor. A lower limit for the scaling factor is given by the concentration course of the M intermediate. For $f_1 = 1.0$ (Figure 5b), the concentration of M is zero in the late-time domain, and it would be negative for smaller scaling factors. Because negative concentrations are clearly unphysical, $f_1 = 1.0$ is a lower limit. A well-defined upper limit cannot be derived from the data, but for $f_2 = 1.2$, the absorbance of N in the short-wavelength range is already considerably smaller than the absorbance of bR (Figure 5a). Larger scaling factors ($f = 1.4$) would even produce negative absorbance for N in this spectral range.

The preceding analysis allows only one N state. The eigenvalue formalism of eq 14 cannot handle the case of two spectroscopically indistinguishable (degenerate) N states. The time dependence of the N anisotropy (Figure 4d) suggests, however, a transition between two substates of the N intermediate, N_1 and N_2, with different time-independent anisotropies, r_{N_1} and r_{N_2}. The time-dependent N anisotropy $r_N(t)$ is then given by

$$r_N(t) = \frac{r_{N_1} n_{N_1}(t) + r_{N_2} n_{N_2}(t)}{n_{N_1}(t) + n_{N_2}(t)}$$

where $n_{N_1}(t)$ and $n_{N_2}(t)$ are the concentrations of N_1 and N_2. Using the constraint that $n_{N_1}(t) + n_{N_2}(t) = n_N(t)$, one of the two concentrations, $n_{N_1}(t)$ or $n_{N_2}(t)$, may be eliminated, and we get

$$n_{N_1}(t) = \frac{n_N(t)(r_N(t) - r_{N_2})}{r_{N_1} - r_{N_2}}$$

The anisotropies r_{N_1} and r_{N_2} are to be chosen so that neither of the partial concentrations $n_{N_1}(t)$ and $n_{N_2}(t)$ becomes negative. This constraint provides a lower limit for the anisotropy of N_1 ($r_{N_1} \geq -0.117$) and an upper limit for the anisotropy of N_2 ($r_{N_2} \leq -0.130$). In between these limits, mathematically any combination of anisotropy values is allowed, and no further constraints are available to determine a unique solution. The time courses for the concentrations of both N substates are shown for two combinations of anisotropies (r_{N_1}, r_{N_2}) in Figure 6. If we choose the limits for both anisotropies ($r_{N_1} = -0.117$ and $r_{N_2} = -0.130$), the concentration of N_2 rises in parallel with the decay of N_1 (Figure 6a), suggesting a sequential pathway. In contrast, for the combination ($r_{N_1} = -0.110$, $r_{N_2} = -0.140$) both substates are simultaneously present during the full time domain (Figure 6b). In the first case, a higher accumulation of each substate was reached.

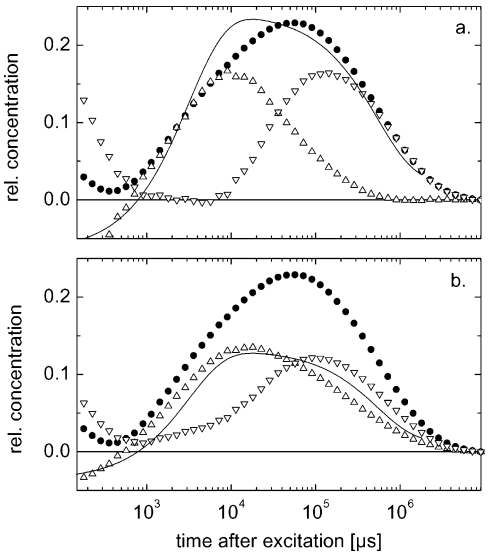

Figure 6. Concentration courses of the two N substates N_1 und N_2 for $r_{N_1} = -0.117$ and $r_{N_2} = -0.130$ (a) and for $r_{N_1} = -0.110$ and $r_{N_2} = -0.140$ (b). ●: N; △: N_1; ▽: N_2; straight line: time course of the fit to the nonabsorptive contribution to the linear birefringence from Figure 3, scaled to fit either N (a) or N_1 (b).

To prove that the measured data require two N substates with different anisotropies, we reconstructed the absorption changes $\Delta A(\lambda, t)$ and the transient linear dichroism $\Delta A(\lambda, t)\, R(\lambda, t)$ according to eqs 5 and 6 and calculated the transient anisotropy $R(\lambda, t)$. In the first case, we used only one N state with the (average) anisotropy $r_N = -0.1238$; in the second case, two N states with identical spectra but different anisotropies ($r_{N_1} = -0.117$ and $r_{N_2} = -0.130$) were assumed. The choice of (r_{N_1}, r_{N_2}) has no influence on the transient anisotropy $R(\lambda, t)$ because for each combination the related time traces $n_{N_1}(t)$ and $n_{N_2}(t)$ have to be recalculated. The result is shown in Figure 7 for the wavelengths that were selected for the determination of the concentration courses. Whereas at 490 nm (Figure 7a) the analysis with two N states shows smaller deviations from the data only until 50 ms, at the other four wavelengths (520, 543, 570, 590 nm) this approach shows excellent agreement with the data (Figure 7b−e) and is clearly superior to the analysis with only one N state that displays large deviations over the considered time range.

In calculating the angles of the transition dipole moment in the transient intermediates with respect to the membrane normal, we use the following anisotropies: $r_M = -0.134 \pm 0.002$, $r_{N_1} = -0.117$, $r_{N_2} = -0.130$, and $r_{bR} = -0.147$. Assuming $\theta_{bR} = 70°$ and a constant second-order parameter S_2, the relation $r_i = r_{bR}/P_2(\cos\theta_{bR}) \cdot P_2(\cos\theta_i)$ yields $\theta_M = 68.4 \pm 0.2°$, $\theta_{N_1} = 66.3°$, and $\theta_{N_2} = 67.9°$. Because of the indefiniteness of the anisotropies, the angle for N_1 is an upper limit, and the angle for N_2 represents a lower limit. The angle for the M state under alkaline conditions is consistent with measurements at neutral pH.[6]

Discussion

Spectral Properties of the N Intermediate. In the present study, the spectrum of the N intermediate in native purple membranes was determined from polarized absorbance changes of an oriented sample that was excited isotropically. The measurements were carried out at pH 10.4 to achieve a sufficiently high accumulation of the N intermediate and a negligible contribution from the O state. From the isotropic absorbance changes and the transient linear dichroism data, an

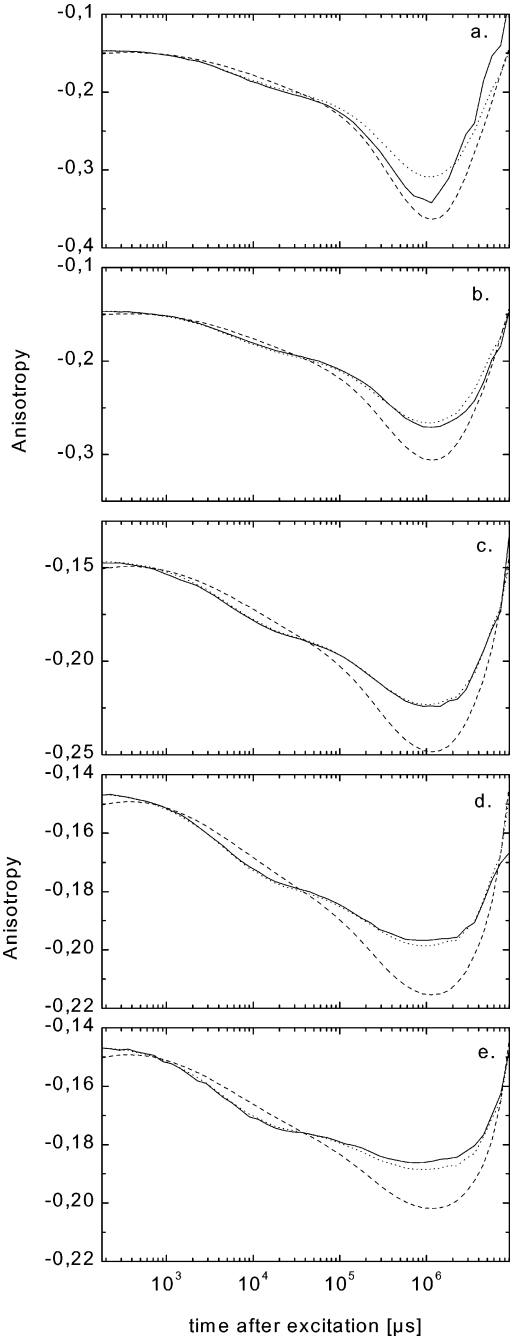

Figure 7. Comparison of the anisotropy time traces at wavelengths $\lambda = 490$ (a), 520 (b), 543 (c), 570 (d), and 590 nm (e). —: data, − − −: approach taking into account only one N state with anisotropy $r_N = -0.1238$, ···: approach taking into account two N states with anisotropies $r_{N_1} = -0.117$ and $r_{N_2} = -0.130$.

eigenvalue equation was derived that yields the spectrum of the N intermediate and the related average anisotropy. No constraints on the shape of the spectrum were required. The limits for the scaling of the spectrum of N were determined empirically. Even at the upper limit ($f = 1.2$) the main absorption band of the N intermediate is associated with a lower oscillator strength with respect to the bR ground state in an all-trans conformation, consistent with a 13-cis conformation of the retinylidene chromophore. At the lower limit ($f = 1.0$), this N spectrum shows overall good agreement with the N spectrum determined from difference spectra during the photocycle over a wide pH range[42] (Figure 8a). As in our approach, in ref 42 no assumptions about the kinetic model entered into the analysis, but various constraints on the shape of the spectra were required.

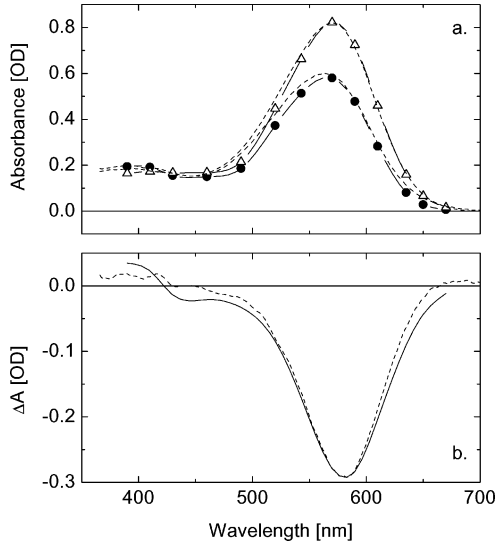

Figure 8. Comparison of the spectra from the transient data of this work (●: N for $|\vec{A}^*_N| = 1$; △: bR) with recent data from ref 42 (− − −). (a) Absorption spectra; (b) N − bR difference spectra (− − −), ref 42; —, spline fit to the data of this work).

Minor (but systematic) deviations occur on the short-wavelength side; these are also present for the related bR spectra. The comparison of the N − bR difference spectra shows that these deviations almost vanish (Figure 8b), indicating that the transient data of the two different experiments are consistent. We note that our steady-state bR spectrum deviates as well from the "transient" bR spectrum on the short-wavelength side (Figure 4a) and is in much better agreement with the bR spectrum in ref 42. Therefore, it is obvious that the deviations for the N spectra are due to different bR spectra. The deviation between the steady-state and the transient bR spectrum suggests that the bR ground state is spectrally heterogeneous at high pH with a noncycling blue-shifted (sub)population.

In a recent study,[43] photocycle data at a number of experimental conditions (temperature, pH, polarization) have been analyzed with a spectrotemporal model. This target analysis uses moderate ("mild") spectral assumptions and a kinetic model with thermodynamic parameters for the microscopic rates. The absorbance of the N intermediate determined in this way is very similar to that in ref 42. In summary, there seems to be a general consensus that the spectrum of the N intermediate ($\lambda_{max} \approx 560$ nm) is only slightly blue-shifted with respect to the bR ground state ($\lambda_{max} \approx 568$ nm) with a considerably smaller extinction coefficient.

Anisotropy and Orientational Changes in N at High pH. Using isotropic excitation of oriented uniaxial PM samples, we measured the transient anisotropy at pH 10.4. Focusing on the M decay, we find that our data are consistent with a sequence of intermediates (M → N_1 → N_2 → bR) with different anisotropies. These anisotropies reflect the orientation of the electronic transition dipole moment with respect to the membrane normal ($r_i = S_2 \cdot P_2(\cos \theta_i)$). Because of uniaxial symmetry, information on changes of the azimuthal angle is not accessible in this kind of experiment. However, the anisotropies are very sensitive to changes in the polar angles θ_i because $dP_2/d\theta_i$ is large for angles near 70°. Assuming that the second-order parameter S_2 does not change during the photocycle, we find the angular changes with respect to the bR ground state to be $\Delta\theta_M = (-1.6 \pm 0.2)°$, $\Delta\theta_{N_1} \leq -3.7°$, and $\Delta\theta_{N_2} \geq -2.1°$ (i.e., the angluar change is at least 3.7° for N_1 and at most 2.1° for N_2). The angular change for the M intermediate under these

conditions is consistent with our previous results[6] determined with wild type and D96A under various conditions (average $\Delta\theta_M = (-1.1 \pm 0.3)°$). In addtion, from a photostationary measurement of D96A at pH 8.0 with nearly 100% M accumulation, we obtained $\Delta\theta_M = (-1.4 \pm 0.3)°$ (data not shown). Therefore, we conclude that the reorientations of the chromophore in the photocycle of bR do not depend significantly on the pH, at least for M. Variations from 10 to 20°, as reported from a photoselection study with isotropic samples,[44] can be clearly ruled out. The changes for the N intermediate are larger than for the early intermediates.[6] Qualitatively, this is consistent with a photoselection study on the mutant T46V/D96N, where the anisotropy of N displayed the largest change with respect to the bR ground state.[45] However, the anisotropy values were not converted into angular changes;[45] therefore, a quantitative comparison is not possible. Moreover, our study is concerned with wild type. Obviously, the changes for the N intermediate determined in the present study are still small enough to fit to the atomic structures of 13-cis conformers determined from X-ray crystallography.[7,8,35,46]

A comparison of various LD experiments and recent X-ray coordinates supports the view that the transition dipole vector approximately connects the C_5 atom of the β-ionone ring with the C_{15} atom.[3,47] The exact orientation of the transition dipole moment within the molecular frame of the chromophore is not known. In ref 48, an angle of 10.5° between the transition dipole moment and the long axis of the chromophore was introduced to reconcile the results from NMR and LD on the chromophore orientation. Because the LD and X-ray results are in good agreement, we see no need to introduce this offset angle. In the meantime, a considerable number of X-ray structures have become available for the bR ground state, and it has become clear that the only discrepancy exists between the X-ray and NMR results, in fact, only for the C_{13} methyl group. This issue of the degree of agreement between results from LD, NMR, and X-ray diffraction was discussed in detail in the review.[3]

By allowing a transient decrease of the second-order parameter S_2, the angular changes would be smaller. As a possible origin of such a decrease, transient changes in the curvature of the membranes could be considered. However, light-scattering experiments have shown that in the gel the membrane is unable to change its curvature (i.e., bending processes associated with the bR photocycle in solution are absent[49−51]). The possibility of significant transient changes of S_2 in our experiments is thus excluded. We note that the interpretation of our anisotropy data does not require the introduction of cooperative phenomena such as membrane bending[52] or the proposed so-called "spectator reorientation model".[44,45,53,54] Moreover, our analysis is not based on assumptions of the kinetic model.

In two previous studies, the anisotropy changes in isotropic PM samples at high pH were measured with partially saturating photoselection.[55,56] Assuming exponential relaxation kinetics, a variety of models were tested[55] that include the reorientation of the chromophore, parallel reactions due to ground-state heterogeneity, cooperativity within a trimer, and branching photocycles. Finally, these authors favored models involving parallel processes and excluding chromophore reorientation between the transient intermediates. However, no value was indicated for the angular change in the transition dipole moment in the excitation (K → bR) and in the recovery of the bR ground state. At least this angular change has to be nonzero; otherwise, the transient anisotropy would be constant.

Similar conclusions were reached in ref 56. From the dependence of the transient dichroic ratio at 412 and 570 nm on the excitation intensity, they proposed that the relative yield of at least two parallel pathways with different dichroic ratios is regulated by a cooperativity among the photocycling molecules. The mechanism of this cooperativity was not specified, and no quantitative information on the reorientation of the transition dipole moment was supplied. The possibility of chromophore reorientations as the only mechanism was ruled out explicitly by these authors.[56]

The two different experimental approaches—isotropic excitation of oriented samples versus partially saturating photoselection of isotropic samples—are not equivalent. The photoselection method used in refs 55 and 56 is rather insensitive to the reorientation of the electronic transition dipole moment. The sensitivity in photoselection is determined by $dP_2/d\theta$ at the small angular change $\Delta\theta_i = \theta_i - \theta_{bR}$, whereas in our method the sensitivity is given by $dP_2/d\theta$ at θ_i itself (see also review ref 3). Typically, the invariance of the anisotropy would allow the reorientation of the chromophore by as much as ±8° within experimental accuracy.[57] The experimental approach used in this study is clearly more appropriate for the detection of the small angular changes that occur. However, we are not able to exclude parallel pathways or cooperativity in the bR photocycle. We re-emphasize that our analysis is model-independent and does not require parallel pathways and cooperative phenomena.

Functional Significance of the $N_1 \rightarrow N_2$ Transition. The time dependence of the anisotropy of the spectrally homogeneous N intermediate reveals a transition between two N substates with different anisotropies in the time range of about 50 ms (Figure 4d). Provided that the second-order parameter S_2 is constant during the photocycle, the anisotropy change from N_1 to N_2 reflects the reorientation of the electronic transition dipole moment by at least $\Delta\theta = +1.6°$. In our previous studies[6] on the early intermediates displaying a 13-cis conformation of the chromophore, we found orientational changes of the same order ($\Delta\theta_L = -1.7°$) with respect to the all-trans ground state. This suggests that the $N_1 \rightarrow N_2$ transition might be associated with the reisomerization of the chromophore. However, time-resolved resonance Raman measurements at pH 9.5 demonstrated that the N intermediate contains a 13-cis,15-anti chromophore.[58] FTIR data show that Asp85 remains fully protonated in the N state[59] even at high pH.[60] The protonated Asp85 and the all-trans conformation of the chromophore would result in a red shift of the spectrum characterizing the O intermediate. Such a red shift was not observed in our measurements, consistent with the assumption of a negligible O contribution in the data analysis. Furthermore, our previous studies on light−dark adaptation showed that the 13-cis isomerization is not necessarily associated with a considerable anisotropy change.[5] Altogether, it is thus not very likely that the retinal in N_2 is in an all-trans conformation.

From photocycle studies of wild-type bR at high pH[52,61−63] and of modified systems with a high accumulation of N,[64−67] at least two N substates were proposed that differ in the protonation state of Asp96.[61,63] Because Asp96 is not in close proximity to the chromophore (≥10 Å), changes in the protonation state of Asp96 are not expected to affect the absorption spectrum in the visible, and the $N_1 \rightarrow N_2$ transition could be spectroscopically silent. Our observation of two spectrally indistinguishable N states would thus be consistent with the above model. From time-resolved ATR/FTIR experiments with wild type, only one N state was reported.[22] The pK_a of Asp96 of 7.1 during the lifetime of N[22] suggests that at pH 10.4 Asp96 remains deprotonated throughout N. The possibility of an N

substate with protonated Asp96 in the recovery of the ground state was not considered,[22] however.

The reorientation of the chromophore between the two N substates in the direction of the initial orientation is very likely associated with a movement of the protonated Schiff base, increasing the distance to Asp96. This configuration may favor the reprotonation of Asp96 from the external medium rather than from the Schiff base. This mechanistic model suggests that the reorientation of the chromophore in the $N_1 \rightarrow N_2$ transition acts as a reprotonation switch for Asp96, stabilizing the protonation state of the Schiff base. Apparently, a two-step reorientation of the chromophore, $M \rightarrow N_1$ and $N_1 \rightarrow N_2$, is required for the irreversible proton uptake by the protein. This scenario is consistent with recent structural data for a late N state[36] (N_2) in which (1) the chromophore is in a 13-cis,15-anti conformation, (2) Asp96 is assumed to be protonated, and (3) the angle of the C_5-C_{15} vector with respect to the membrane normal is only slightly smaller than in the bR ground state.

Nonabsorptive Contribution to Linear Birefringence Associated with N May Be Due to an Electric Field Effect. A comparison of the experimentally determined birefringence changes $\Delta\Delta n(\lambda, t)$ with the Kramers−Kronig transform of the linear dichroism data revealed the existence of a wavelength-independent contribution that is apparently not related to absorption changes (Figure 2b). The time course of this contribution (rise and decay times 3 ms/500 ms, see Figure 3) is redrawn in Figure 6, where it may be compared with the kinetics of the N intermediate. The comparison suggests that these two signals are correlated in time. The nonabsorptive LB signal could be correlated either with the total concentration of N (Figure 6a) or with the concentration of N_1 (Figure 6b). We cannot distinguish between these possibilities because of the uncertainty in the r_{N_1} and r_{N_2} values. This argument is supported by measurements under conditions of very low N accumulation (such as in wild type at neutral pH as well as in the mutant D96A), where no wavelength-independent contributions to the LB were observed in the decay of M (data not shown).

A very straightforward explanation of the correlation with the N intermediate would be a transient curvature of the membranes due to lateral pressure induced by hydration in the cytoplasmic region of the protein, as suggested by Váró and Lanyi.[52] Bending of the membranes would clearly produce changes in form and intrinsic birefringence due to a change in the second-order parameter S_2.[5] Additionally, bending would be accompanied by stress birefringence. As discussed above, transient bending of membranes immobilized in a gel can be excluded. On the basis of light-scattering experiments in suspension,[51] these bending processes display only small amplitudes at high pH, anyway.

The magnetically oriented purple membranes are uniaxial and exhibit considerable intrinsic linear birefringence in the dark.[5] This intrinsic LB may change in time because of transient electric fields that develop during the photocycle when protons are transported and donor and acceptor groups change their charge states. Such electrooptical field effects are well known (e.g., Pockels effect). In the M to N transition, a proton is transferred from Asp96 to the Schiff base, generating a negative charge at Asp96. The associated transient field in the low-dielectric membrane has the right order of magnitude (10^5 V/cm)[68,69] to generate the observed change in LB. The strong voltage dependence of the steady-state current is attributed to the millisecond step in the charge displacement (i.e., the reprotonation of the Schiff base from Asp96[69]). Further evidence for the occurrence of a strong electric field in this time domain comes from time-resolved photovoltage measurements with double-flash excitation.[68] Because of the voltage dependence of the rate constant, the kinetics of the millisecond charge displacement induced by the second flash (532 nm) is strongly slowed by the electric field built up by the first flash (580 nm). The charge on Asp96 disappears again during the decay of N when Asp96 is reprotonated from the external medium[10,70] or in the transition between N_1 and N_2 (as discussed in the previous section). This explains the correlation between the transient wavelength-independent LB and the concentration of the N intermediate (or N_1 intermediate). At neutral pH and in the D96A mutant where not enough N accumulates, the rise and decay time constants are very similar, explaining why no such LB effect is observed. In the time range considered in this paper, the transient charge change of Asp96 is the largest source for a transient field effect. In the earlier time range, additional charge changes occur, such as the protonation of Asp85 in the formation of M. The associated smaller transient fields may be responsible for the small, possibly negative $\Delta\Delta n$ around 10−100 μs. However, in double-flash experiments, no significant electric field effect was observed on the electrical component associated with the rise of M.[68]

As an alternative explanation, we propose that the nonabsorptive contribution to linear birefringence is associated with large conformational changes on the cytoplasmic side of the protein. According to an electron cryocrystallography study on the N intermediate of the mutant F219L,[15] these changes involve an extraordinarily large outward tilt of helix F together with helix E, which opens a water-accessible channel. However, recent time-resolved UV resonance Raman experiments suggest that the tilt of helix F occurs in the $M_1 \rightarrow M_2$ transition preceding the invasion of water molecules in the formation of the N intermediate.[21] On the other hand, the kinetic correlation of the nonabsorptive LB contribution with the concentration of N and the reorientation of the chromophore toward the cytoplasmic side in our experiment suggests that the nonabsorptive LB reflects the structural rearrangements in the cytoplasmic region induced by the tilt of helix F. The interaction between helix F and the retinylidene chromophore is mediated by the indole ring of Trp182 and the 13-methyl group[2,71] and/or the 9-methyl group[66] of the chromophore. This tight steric coupling is lost when the chromophore reorients in the $N_1 \rightarrow N_2$ transition moving away from the cytoplasmic side. The reversal of the conformational change of the protein as indicated by the decay of the nonabsorptive LB contribution appears concomitantly with the decay of N_2 and the recovery of the bR ground state. However, the very recently solved crystal structure of a photostationary N intermediate that likely refers to our N_2 does not display large-scale conformational changes on the cytoplasmic side of the membrane.[36] A high-resolution crystallographic structure of an early N state (N_1) that occurs in a sequential pathway in the M decay[36] remains to be determined and may clarify the validity of our proposed molecular model.

Acknowledgment. We thank one of the reviewers for his critical comments which led to improvements in the derivation of the eigenvalue equation. This research was supported by the Deutsche Forschungsgemeinschaft, grant He1382/7-2 and the Ständige Kommission für Forschung und Wissenschaftlichen Nachwuchs (FNK), Freie Universität Berlin, grant 02/524 01.

References and Notes

(1) Braiman, M. S.; Mathies, R. A. *Proc. Natl. Acad. Sci. U.S.A.* **1982**, *79*, 403−407.

(2) Lanyi, J. K. *J. Phys. Chem. B* **2000**, *104*, 11441−11448.

(3) Heyn, M. P.; Borucki, B.; Otto, H. *Biochim. Biophys. Acta* **2000**, *1460*, 60−74.
(4) Otto, H.; Zscherp, C.; Borucki, B.; Heyn, M. P. *J. Phys. Chem.* **1995**, *99*, 3847−3853.
(5) Borucki, B.; Otto, H.; Heyn, M. P. *J. Phys. Chem. B* **1998**, *102*, 3821−3829.
(6) Borucki, B.; Otto, H.; Heyn, M. P. *J. Phys. Chem. B* **1999**, *103*, 6371−6383.
(7) Luecke, H.; Richter, H. T.; Lanyi, J. K. *Science* **1998**, *280*, 1934−1937.
(8) Luecke, H.; Schobert, B.; Richter, H. T.; Cartailler, J. P.; Lanyi, J. K. *Science* **1999**, *286*, 255−261.
(9) Holz, M.; Drachev, L. A.; Mogi, T.; Otto, H.; Kaulen, A. D.; Heyn, M. P.; Skulachev, V. P.; Khorana, H. G. *Proc. Natl. Acad. Sci. U.S.A.* **1989**, *86*, 2167−2171.
(10) Otto, H.; Marti, T.; Holz, M.; Mogi, T.; Lindau, M.; Khorana, H. G.; Heyn, M. P. *Proc. Natl. Acad. Sci. U.S.A.* **1989**, *86*, 9228−9232.
(11) Kamikubo, H.; Kataoka, M.; Váró, G.; Oka, T.; Tokunaga, F.; Needleman, R.; Lanyi, J. K. *Proc. Natl. Acad. Sci. U.S.A.* **1996**, *93*, 1386−1390.
(12) Oka, T.; Yagi, N.; Fujisawa, T.; Kamikubo, H.; Tokunaga, F.; Kataoka, M. *Proc. Natl. Acad. Sci. U.S.A.* **2000**, *97*, 14278−14282.
(13) Steinhoff, H.-J.; Mollaaghababa, R.; Altenbach, C.; Hideg, K.; Krebs, M.; Khorana, H. G.; Hubbell, W. L. *Science* **1994**, *266*, 105−107.
(14) Thorgeirsson, T. E.; Xiao, W.; Brown, L. S.; Needleman, R.; Lanyi, J. K.; Shin, Y. K. *J. Mol. Biol.* **1997**, *273*, 951−957.
(15) Vonck, J. *EMBO J.* **2000**, *19*, 2152−2160.
(16) Pfefferlé, J.-M.; Maeda, A.; Sasaki, J.; Yoshizawa, T. *Biochemistry* **1991**, *30*, 6548−6556.
(17) Souvignier, G.; Gerwert, K. *Biophys. J.* **1992**, *63*, 1393−1405.
(18) Rothschild, K. J.; Marti, T.; Sonar, S.; He, Y.-W.; Rath, P.; Fischer, W.; Khorana, H. G. *J. Biol. Chem.* **1993**, *268*, 27046−27052.
(19) Lazarova, T.; Padrós, E. *Biochemistry* **1996**, *35*, 8354−8358.
(20) Zscherp, C.; Heberle, J. *J. Phys. Chem. B* **1997**, *101*, 10542−10547.
(21) Hashimoto, S.; Sasaki, M.; Takeuchi, H.; Needleman, R.; Lanyi, J. K. *Biochemistry* **2002**, *41*, 6495−6503.
(22) Zscherp, C.; Schlesinger, R.; Tittor, J.; Oesterhelt, D.; Heberle, J. *Proc. Natl. Acad. Sci. U.S.A.* **1999**, *96*, 5498−5503.
(23) Xiao, W.; Brown, L. S.; Needleman, R.; Lanyi, J. K.; Shin, Y. K. *J. Mol. Biol.* **2000**, *304*, 715−721.
(24) Sasaki, J.; Shichida, Y.; Lanyi, J. K.; Maeda, A. *J. Biol. Chem.* **1992**, *267*, 20782−20786.
(25) Kamikubo, H.; Oka, T.; Imamoto, Y.; Tokunaga, F.; Lanyi, J. K.; Kataoka, M. *Biochemistry* **1997**, *36*, 12282−12287.
(26) Sass, H. J.; Schachowa, I. W.; Rapp, G.; Koch, M. H.; Oesterhelt, D.; Dencher, N. A.; Büldt, G. *EMBO J.* **1997**, *16*, 1484−1491.
(27) Rödig, C.; Siebert, F. *FEBS Lett.* **1999**, *445*, 14−18.
(28) Oka, T.; Yagi, N.; Tokunaga, F.; Kataoka, M. *Biophys. J.* **2002**, *82*, 2610−2616.
(29) Hu; J. G.; Sun, B. Q.; Bizounok, M.; Hatcher, M. E.; Lansing, J. C.; Raap, J.; Verdegem, P. J.; Lugtenburg, J.; Griffin R. G.; Herzfeld, J. *Biochemistry* **1998**, *37*, 8088−8096.
(30) Subramaniam, S.; Lindahl, M.; Bullough, P.; Faruqi, A. R.; Tittor, J.; Oesterhelt, D.; Brown, L.; Lanyi, J.; Henderson, R. *J. Mol. Biol.* **1999**, *287*, 145−161.
(31) Sass, H. J.; Büldt, G.; Gessenich, R.; Hehn, D.; Neff, D.; Schlesinger, R.; Berendzen, J.; Ormos, P. *Nature* **2000**, *406*, 649−653.
(32) Subramaniam, S.; Henderson, R. *Nature* **2000**, *406*, 653−657.
(33) Rink, T.; Pfeiffer, M.; Oesterhelt, D.; Gerwert, K.; Steinhoff, H. J. *Biophys. J.* **2000**, *78*, 1519−1530.
(34) Radzwill, N.; Gerwert, K.; Steinhoff, H.-J. *Biophys. J.* **2001**, *80*, 2856−2866.
(35) Lanyi, J. K.; Schobert, B. *J. Mol. Biol.* **2002**, *321*, 727−737.
(36) Schobert, B.; Brown, L. S.; Lanyi, J. K. *J. Mol. Biol.* **2003**, *330*, 553−570.
(37) Váró, G.; Lanyi, J. K. *Biochemistry* **1990**, *29*, 2241−2250.
(38) Váró, G.; Duschl, A.; Lanyi, J. K. *Biochemistry* **1990**, *29*, 3798−3804.
(39) Groma, G. I.; Bogomolni, R. A.; Stoeckenius, W. *Biochim. Biophys. Acta* **1997**, *1319*, 59−68.
(40) Henry, E. R.; Hofrichter, J. *Methods Enzymol.* **1992**, *210*, 129−192.
(41) Hendler, R. W.; Shrager, R. I. *J. Biochem. Biophys. Methods* **1994**, *28*, 1−33.
(42) Gergely, C.; Zimányi, L.; Váró, G. *J. Phys. Chem. B* **1997**, *101*, 9390−9395.
(43) van Stokkum, I. H. M.; Lozier, R. H. *J. Phys. Chem. B* **2002**, *106*, 3477−3485.
(44) Harms, G. S.; Song, Q.; Johnson, C. K. *Biophys. J.* **1996**, *70*, 2352−2357.
(45) Harms, G. S.; Johnson, C. K. *Photochem. Photobiol.* **1997**, *66*, 133−139.
(46) Schobert, B.; Cupp-Vickery, J.; Hornak, V.; Smith, S. O.; Lanyi, J. K. *J. Mol. Biol.* **2002**, *321*, 715−726.
(47) Lin, S. W.; Mathies, R. A. *Biophys. J.* **1989**, *56*, 653−660.
(48) Hudson, S.; Birge, R. R. *J. Phys. Chem. A* **1999**, *103*, 2274−2281.
(49) Czégé, J. *FEBS Lett.* **1988**, *242*, 89−93.
(50) Czégé, J.; Reinisch, L. *Biophys. J.* **1990**, *58*, 721−729.
(51) Czégé, J.; Reinisch, L. *Photochem. Photobiol.* **1991**, *54*, 923−930.
(52) Váró, G.; Needleman, R.; Lanyi, J. K. *Biophys. J.* **1996**, *70*, 461−467.
(53) Ahl, P. L.; Cone, R. A. *Biophys. J.* **1984**, *45*, 1039−1049.
(54) Wan, C.; Qian, J.; Johnson, C. K. *Biophys. J.* **1993**, *65*, 927−938.
(55) Groma, G. I.; Bogomolni, R. A.; Stoeckenius, W. *Biochim. Biophys. Acta* **1997**, *1319*, 69−85.
(56) Tokaji, Z.; Dancsházy, Z. *Biochem. Biophys. Res. Commun.* **1997**, *233*, 532−536.
(57) Esquerra, R. M.; Che, D.; Shapiro, D. B.; Lewis, J. W.; Bogomolni, R. A.; Fukushima, J.; Kliger, D. S. *Biophys. J.* **1996**, *70*, 962−970.
(58) Fodor, S. P.; Ames, J. B.; Gebhard, R.; van den Berg, E. M.; Stoeckenius, W.; Lugtenburg, J.; Mathies, R. A. *Biochemistry* **1988**, *27*, 7097−7101.
(59) Bousché, O.; Sonar, S.; Krebs, M. P.; Khorana, H. G.; Rothschild, K. J. *Photochem. Photobiol.* **1992**, *56*, 1085−1095.
(60) Braiman, M. S.; Dioumaev, A. K.; Lewis, J. R. *Biophys. J.* **1996**, *70*, 939−947.
(61) Ames, J. B.; Mathies, R. A. *Biochemistry* **1990**, *29*, 7181−7190.
(62) Cao, Y.; Váró, G.; Klinger, A. L.; Czajkowsky, D. M.; Braiman, M. S.; Needleman, R.; Lanyi, J. K. *Biochemistry* **1993**, *32*, 1981−1990.
(63) Zimányi, L.; Cao, Y.; Needleman, R.; Ottolenghi, M.; Lanyi, J. K. *Biochemistry* **1993**, *32*, 7669−7678.
(64) Delaney, J. K.; Schweiger, U.; Subramaniam, S. *Proc. Natl. Acad. Sci. U.S.A.* **1995**, *92*, 11120−11124.
(65) Weidlich, O.; Friedman, N.; Sheves, M.; Siebert, F. *Biochemistry* **1995**, *34*, 13502−13510.
(66) Weidlich, O.; Schalt, B.; Friedman, N.; Sheves, M.; Lanyi, J. K.; Brown, L. S.; Siebert, F. *Biochemistry* **1996**, *35*, 10807−10814.
(67) Dioumaev, A. K.; Brown, L. S.; Needleman, R.; Lanyi, J. K. *Biochemistry* **2001**, *40*, 11308−11317.
(68) Dickopf, S.; Heyn, M. P. *Biophys. J.* **1997**, *73*, 3171−3181.
(69) Braun, D.; Dencher, N. A.; Fahr, A.; Lindau, M.; Heyn, M. P. *Biophys. J.* **1988**, *53*, 617−621.
(70) Bousché, O.; Braiman, M.; He, Y.-W.; Marti, T.; Khorana, H. G.; Rothschild, K. J. *J. Biol. Chem.* **1991**, *266*, 11063−11067.
(71) Moltke, S.; Wallat, I.; Sakai, N.; Nakanishi, K.; Brown, M. F.; Heyn, M. P. *Biochemistry* **1999**, *38*, 11762−11772.